Development of a small animal PET/MRI insert

Aaron R. Selfridge and Felipe Godinez
Department of Radiology, University of California, Davis
Email: arselfridge@ucdavis.edu

Introduction

We have developed a high sensitivity, high resolution preclinical PET insert for a Bruker Biospec 7T MRI system. This system targets whole body mouse or rat brain studies, particularly where dynamic PET and MRI must be acquired simultaneously. Increased PET sensitivity allows for shorter imaging frames and better quantitation, both of which are especially relevant to analysis of dynamic data and kinetic modeling. Furthermore, improvements in sensitivity must be met without compromising spatial resolution to ensure that mouse and rat physiology is imaged with enough detail.

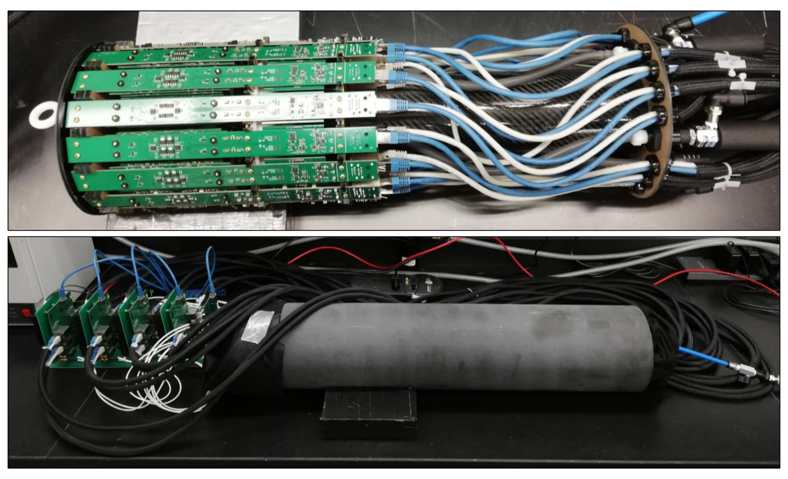

Figure 1: Image of the PET insert without (top) and with (bottom) the outer cover

PET Insert Design

Detector

Each PET detector module used in the system includes four LYSO crystal arrays with 19x19 elements and 1.0 mm crystal pitch. Each array is 20 mm long with a diffuse reflector and dual-ended readout providing depth-of-interaction encoding.

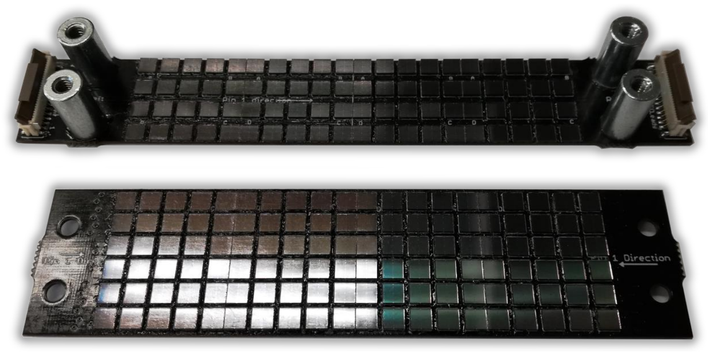

Figure 2: Front and rear SiPM arrays used for dual ended readout

Electronics

Custom readout electronics interface between the analog output of the photodetector and the acquisition computer. The readout utilizes a linearized time-over-threshold circuit, producing one pulse-width-modulated digital signal per channel. An FPGA receives digitized signals from the four blocks in each module, produces single events, and transfers them to a computer.

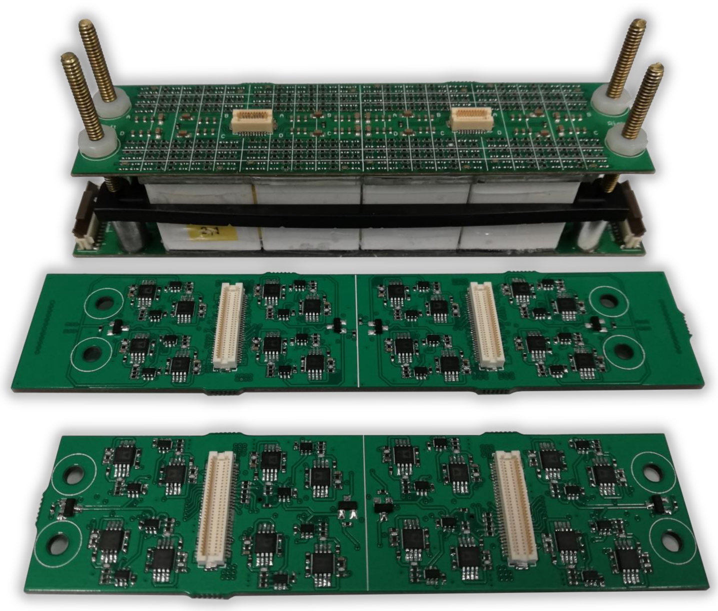

Figure 3: Module containing four block coupled to SiPM arrays, and readout boards

System

The system has an axial field-of-view (FOV) of approximately 8 cm and accommodates RF coils with diameter up to 9 cm. The system electronics are cooled using chilled air generated by multiple vortex tubes, with RF shielding provided by two carbon fiber tubes.

Figure 4: Two modules used to acquire coincidences, mounted on laser cut Delrin rings.

System Characterization

Detector performance was evaluated based on energy and timing resolution, as well as separation of crystal elements. Two detector modules were irradiated with a ^{22}Na point source and single event data were acquired. Singles floods were segmented and used to assess crystal separability. Singles were sorted into coincidences and used to assess energy and timing resolution. Point source and Derenzo phantom images were acquired and reconstructed to evaluate preliminary system imaging performance.

MRI compatibility of system electronics and detectors was assessed by acquiring gradient and spin echo images without any system components, with only electronics, and with electronics and one detector module.

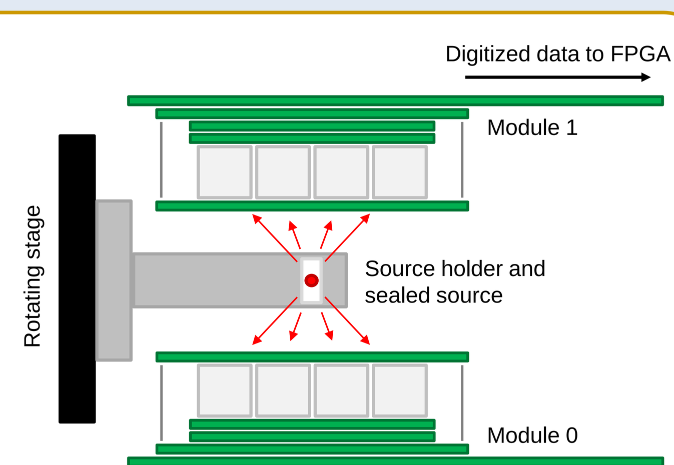

Figure 5: Schematic showing two modules positioned for coincidence and image acquisition

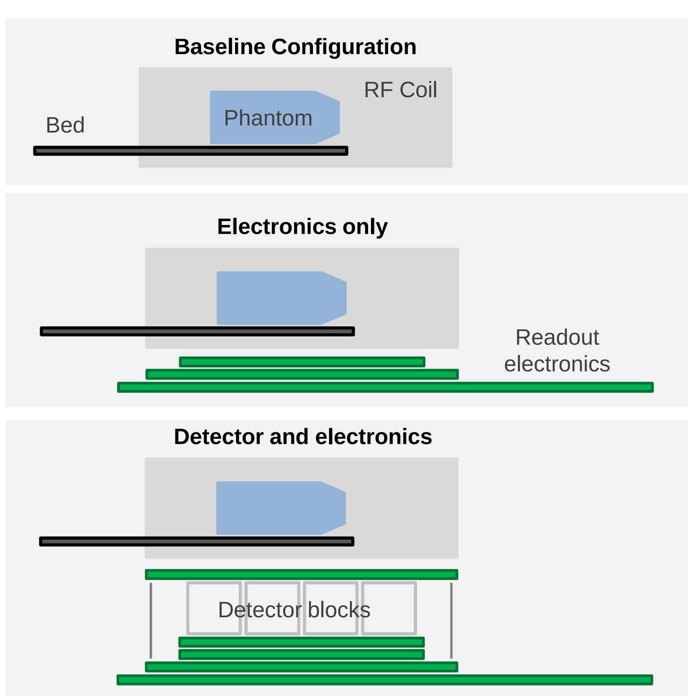

Figure 6: Three configurations used to acquire MRI images

Detector Characterization

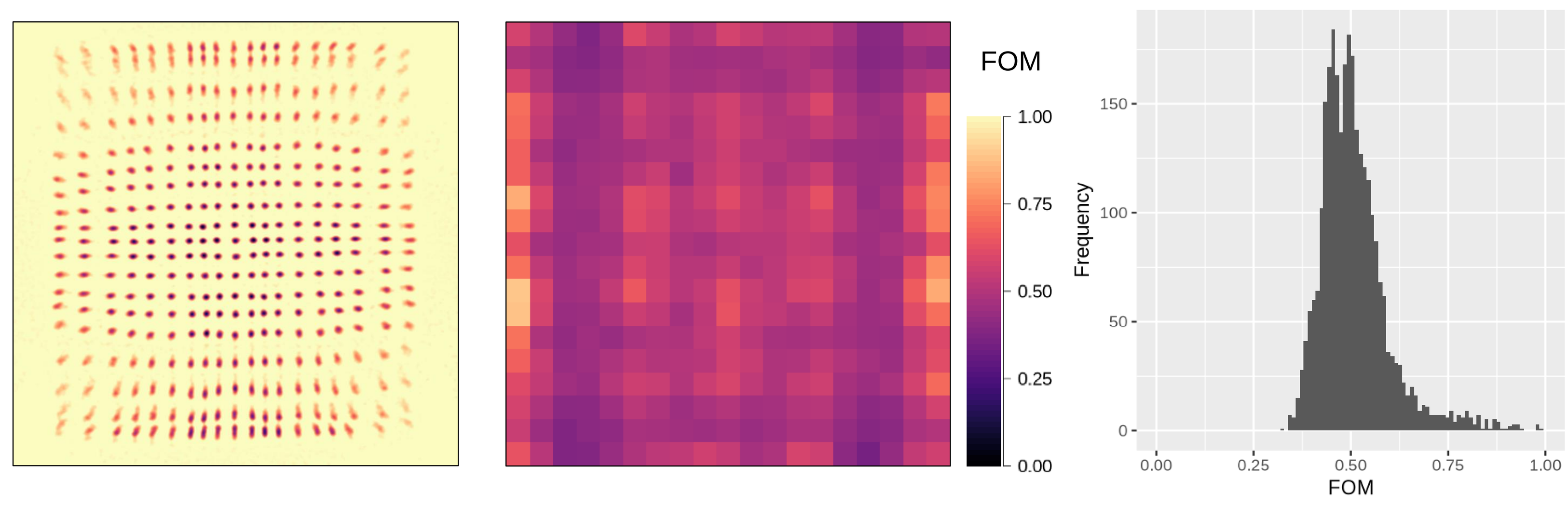

Figure 7: (Left) Laplacian of a Gaussian filtered singles flood histogram from one block. (Middle) Figure of merit (FOM) for each crystal in the unfiltered flood, calculated as the width of each peak divided by the mean distance to its neighbors. (Right) Histogram of FOM for all eight blocks in the system.

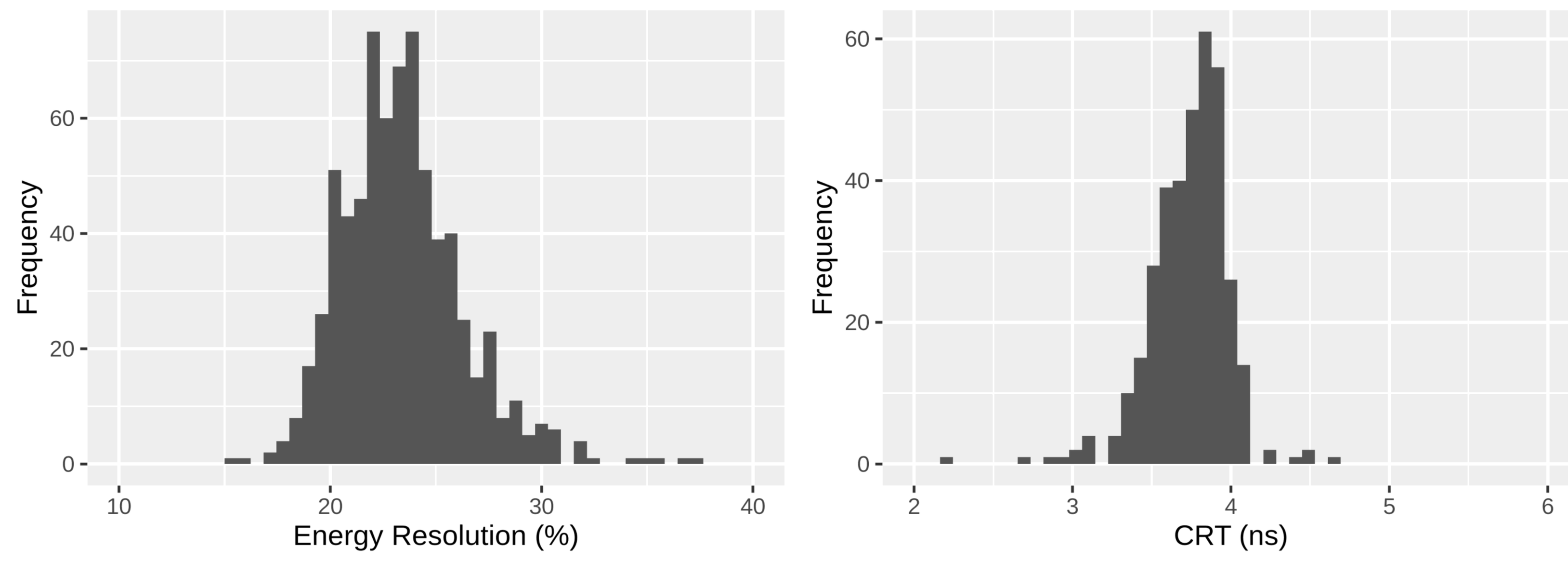

Figure 8: (Left) Histogram of energy resolution for each crystal in one block. (Right) Histogram of timing resolution for each crystal in one block, in coincidence with any crystal in an opposing block. No DOI correction was applied to either measure

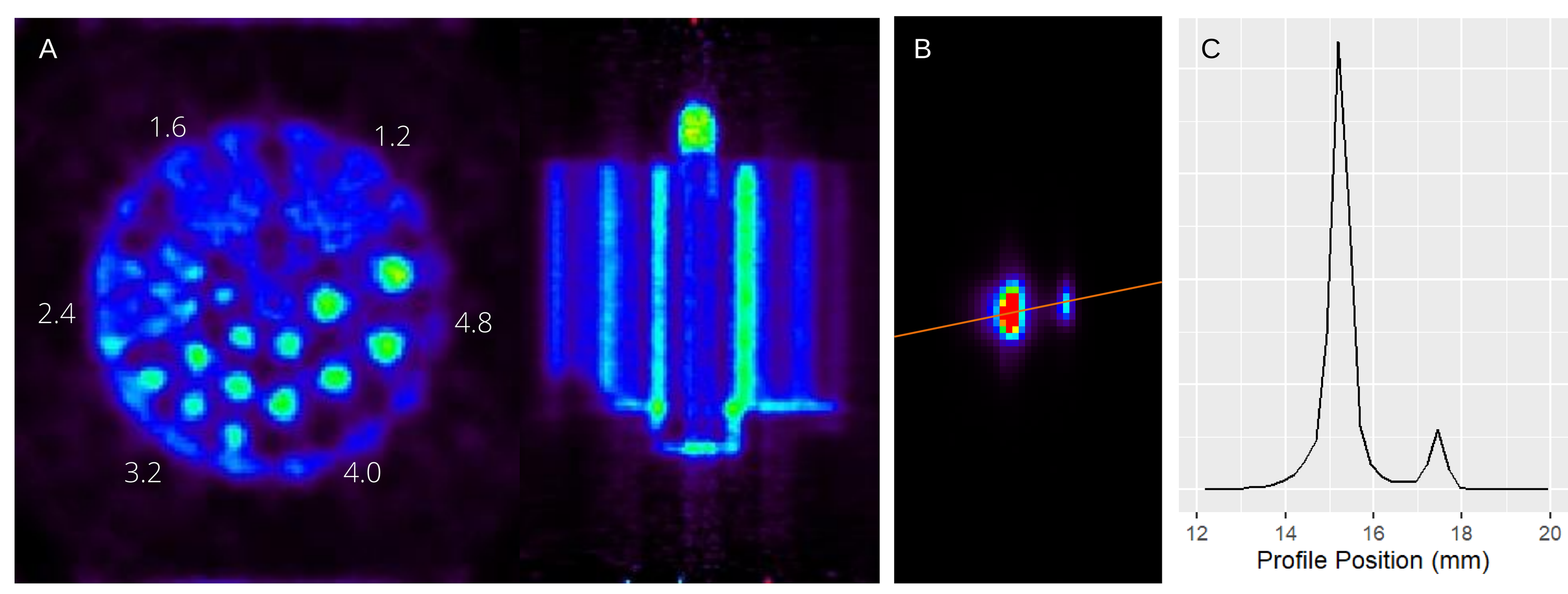

Figure 9: (A) Reconstructed Derenzo phantom showing rod size in mm. (B) Reconstructed image showing point sources with different activity. (C) Line profile through the point sources.

MRI Compatibility

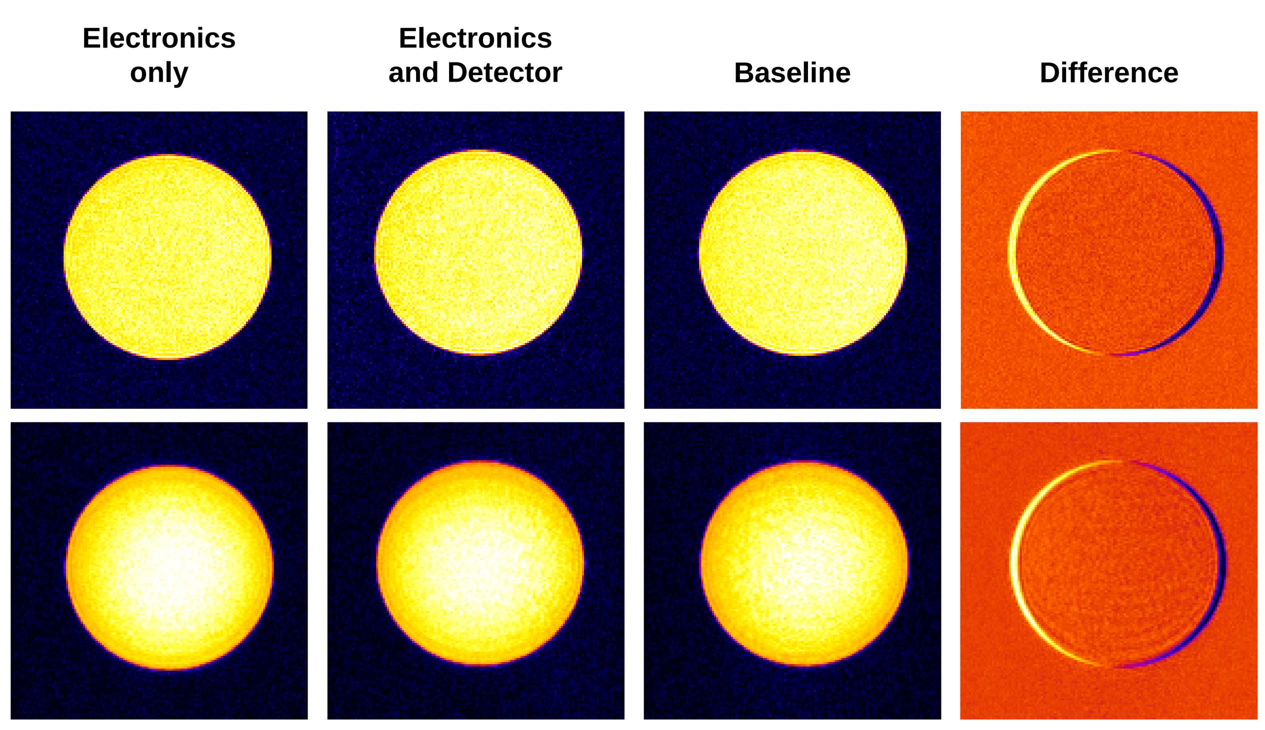

Figure 10: Spin (top) and gradient (bottom) echo images showing the three configurations. Difference images reflect changes between the baseline and images acquired with both detector and electronics.

PET insert components introduce only minor changes in the gradient echo images, which are more susceptible than spin echo images to changes in B_0.

Conclusion

Based on the initial performance results, we expect that the complete system will be well suited for regular use in a variety of applications. Mean energy and timing resolutions were 23% and 3.7ns. Initial imaging results demonstrates that fundamental system functions such as signal readout and detector synchronization do not introduce errors which are clearly manifest in sinograms or reconstructed images. Additionally, the PET insert components show minimal impact on MRI performance, despite the presence of amplifiers, power regulators, and FPGAs.

Funding Sources
This work was funded by NIH grant 5R01EB021395.

Department of Radiology

UC DAVIS UNIVERSITY OF CALIFORNIA

center for molecular and genomic imaging cmgi